JOC The Journal of Organic Chemistry

FEATURED ARTICLE

pubs.acs.org/joc

Stictamides A−C, MMP12 Inhibitors Containing 4-Amino-3-hydroxy-5-phenylpentanoic Acid Subunits

Zhibin Liang,[†] Analia Sorribas,[†] Florian J. Sulzmaier,[⊥] Jorge I. Jiménez,[∥] Xin Wang,[‡] Thomas Sauvage,[§] Wesley Y. Yoshida,[†] Guangyi Wang,[‡] Joe W. Ramos,[⊥] and Philip G. Williams*[,†,⊥]

[†]Departments of Chemistry, [‡]Oceanography, and [§]Botany, University of Hawaii at Manoa, Honolulu, Hawaii 96822, United States

[⊥]University of Hawaii Cancer Center, 651 Ilalo Street, Honolulu, Hawaii 96813, United States

[∥]AgraQuest, Inc., 1540 Drew Avenue, Davis, California 95618, United States

Supporting Information

ABSTRACT: An extensive study of the secondary metabolites produced by a new *Sticta* sp. of lichen has led to the isolation of three new compounds containing the 4-amino-3-hydroxy-5-phenylpentanoic acid residue (Ahppa). The structures of stictamides A−C (**1**−**3**) were assigned by 2D NMR spectroscopic and chemical methods. Due to extensive epimerization of the Ahppa residue observed after acid hydrolysis, the configuration of this unit was deduced through conversion of **1** to an appropriate derivative and application of our recently developed statine NMR database. Evaluation of stictamide A against a panel of disease-relevant proteases showed that it inhibited MMP12 at 2.3 μM and significantly reduced invasion in the human glioma cell line U87MG. Docking studies suggest that stictamide A inhibits MMP12 by a non-zinc-binding mechanism.

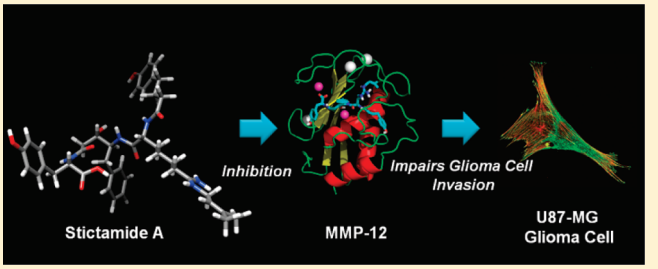

INTRODUCTION

Statine-like amino acids are a well-known motif in natural products. Originally identified as a residue in the classic protease inhibitor pepstatin,[1] the biosynthesis of these γ-amino-β-hydroxy acids involves the condensation of a protogenic amino acid with malonate via an oxidative decarboxylation reaction.[2] The unit has attracted considerable interest as natural products containing this moiety have been reported to display a wide spectrum of biological activities ranging from anticancer[3] to the inhibition of P-glycoprotein efflux pumps.[4] As statine moieties function as peptide isosteres, being transition state mimics of peptide hydrolysis,[5] they are common design elements in protease inhibitors.[6] Incorporation of this residue can significantly improve the pharmacokinetic properties and potency of that class of compounds. As part of a general screening program for protease inhibitors, an extract derived from a new *Sticta* sp. (Order Peltigerales: Family Lobariaceae) of lichen was identified which showed protease inhibition in our initial screens. Fractionation of the extract has now led to the identification of three statine-containing peptides, stictamides A−C (**1**−**3**). We report here their isolation and structure determination. In addition, we report the protease profiling and evaluation of the effect of **1** on invasion of U87-MG, a human glioblastoma cell line, and its viability.

RESULTS AND DISCUSSION

Stictamide A (**1**) was isolated as an optically active light yellow powder ($[\alpha]_D$ −0.2 (*c* 0.2, MeOH)). The molecular weight of **1**

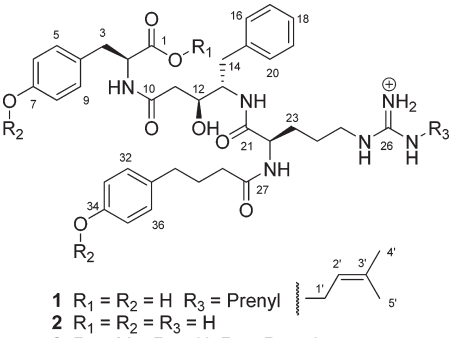

was obtained from the mass spectrum, which showed a molecular ion peak at *m*/*z* 759.4082 $[M]^+$. On the basis of HR-ESI-TOFMS data, the molecular formula was defined as $C_{41}H_{55}N_6O_8$, which indicated that **1** contained 18 double bond equivalents and a positive charge. In total, 35 carbon resonances were observed in the ^{13}C NMR and multiplicity-edited HSQC spectra, suggesting that elements of symmetry were present in the compound. On the basis of the number of sp^2 carbons and their chemical shifts, these symmetry elements were assigned to one mono- and two disubstituted phenyl rings. The 41 carbons required by the molecular formula could therefore be ascribed to 11 quaternary, 18 methine, 10 methylene, and 2 methyl carbons.

Received: February 1, 2011
Published: April 18, 2011

 © 2011 American Chemical Society

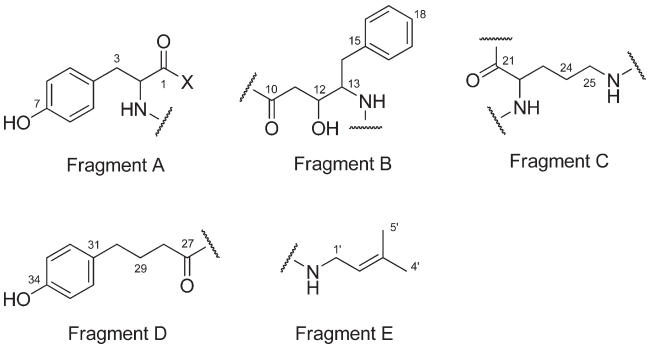

Figure 1. Initial fragments assembled from analyses of the 2D NMR data.

These could be further assigned as five carbon−heteroatom double bonds ($\delta_{C\text{-}1}$ 178.9; $\delta_{C\text{-}10}$ 172.5; $\delta_{C\text{-}21}$ 174.3; $\delta_{C\text{-}26}$ 157.3; $\delta_{C\text{-}27}$ 175.9) and 10 carbon−carbon double bonds that accounted for 15 of the total 18 degrees of unsaturation implied by the molecular formula. This indicated that **1** contained three rings.

Analysis of the spectroscopic data established the units that constituted **1**. Briefly, HMBC correlations from a pair of diastereotopic benzylic protons ($\delta_{H\text{-}3}$ 3.13 and 2.86) to a *para*-substituted aromatic ring, a downfield methine ($\delta_{C\text{-}2}$ 57.8), and a carbonyl carbon ($\delta_{C\text{-}1}$ 178.9) established the presence of a tyrosine moiety (fragment A). A second unit (fragment B) could be established beginning with the carbinol proton signal (H-12) at δ_H 4.08. This proton resonance displayed TOCSY correlations to a methine proton signal at δ_H 4.10 (H-13) and showed COSY cross peaks to methylene proton signals at $\delta_{H\text{-}11}$ 2.39 and 2.29 that, in conjunction with HMBC correlations from H-12 to C-11, from H-14 to C-13, and from H-14 to C-15, indicated this fragment was 4-amino-3-hydroxy-5-phenylpentanoic acid (Ahppa; fragment B). One-dimensional TOCSY experiments defined a continuous four-carbon spin system composed of three methylenes and one methine (C-22 to C-25) that was built into fragment C. The downfield chemical shift of the carbons at each end ($\delta_{C\text{-}22}$ 54.5; $\delta_{C\text{-}25}$ 41.9) indicated that these carbons were adjacent to nitrogen atoms, while the HMBC correlation from the proton attached to C-22 to the carbonyl carbon C-21 indicated that fragment C was ornithine. Fragment D evidently contained a second *para*-substituted phenyl ring, based on the characteristic AB system ($\delta_{H\text{-}32}$ 6.99 d, 8.4 Hz; $\delta_{H\text{-}33}$ 6.68 d, 8.4 Hz) visible in the ^{1}H NMR spectrum. This spin system could be attached on the basis of a series of HMBC correlations to the terminal end of an *n*-butanoic acid unit, thus defining the 4-(4-hydroxyphenyl)butanoic acid residue (fragment D). The final unit (fragment E) contained two methyl singlets with proton chemical shifts indicative of attachment to a sp^2 carbon. HMBC correlations from these methyl groups to each other and to two sp^2 carbons, which also were coupled to a methylene carbon, defined this unit as a prenyl moiety.

HMBC correlations provided the final carbon−carbon connectivities. Fragment B (Ahppa) was linked to the nitrogen atom of fragment A (Figure 1) by an HMBC correlation from H-2 to C-10. Fragment C was located between the amino terminus of Ahppa and C-27 of fragment D based on HMBC correlations from H-13 to C-21 and H-22 to C-27. Finally, the last remaining carbon C-26 at δ_C 157.3 was linked to fragments C and E via the remaining nitrogen atoms, on the basis of HMBC correlations observed from both H-25 and H-1′ to C-26. Two functional groups were still possible for this sp^2 carbon (C-26) that would result in **1** containing either an *N*′-prenylarginine or an *N*′-prenylcitrulline unit, with a carboxylic acid or primary amide, respectively, at C-1. These two possible structures could not be conclusively distinguished via the IR spectrum nor could they be distinguished via a chemical shift argument.

In the end, this required the treatment of a 500 μg sample of **1** with trimethylsilyldiazomethane to determine whether C-1 was a carboxylic acid or a primary amide. The progress of the reaction was monitored by LC-MS analysis (Figure 2), which after an hour indicated a complex mixture of mono-, di-, and trimethylated products that slowly coalesced over the next 2.5 h into one major product (**4**) corresponding to the trimethylated derivative (m/z 801.4547 $[M]^+$). To confirm that methylation occurred exclusively at the phenolic and carboxylic acid oxygens, the product was isolated and the proton spectrum recorded. The ^{1}H NMR spectrum of the isolated product was essentially identical to the starting material except for two additional methoxy singlets at δ_H 3.65 and δ_H 3.73 integrating to 3 and 6, respectively (see Supporting Information Figure S12). Analysis of the HMBC spectrum of this derivative indicated that the two methyl signals at δ_H 3.73 showed clear correlations to *O*-arylcarbons at approximately δ_C 159.0, while the methoxy signal at δ_H 3.65 clearly correlated to a carbonyl carbon at δ_C 173.0 (see Supporting Information Figure S13), establishing conclusively that C-1 in **1** was a carboxylic acid and unit C contained a guanidine rather than a carbamate functional group. Analysis of the MS/MS fragmentation pattern provided additional data to support this assignment (vide infra).

Detailed LC-MS analyses of the initial column fractions led to the identification of two analogues. Subsequent isolation and characterization of the more polar metabolite **2** indicated that **1** and **2** possessed similar structures, although a comparison of the high-resolution ESI-TOF data established that **2** ($C_{36}H_{47}N_6O_8$) was 68 amu smaller than **1**. This mass difference was easily explained after the observation that the two allylic methyl resonances in the ^{1}H NMR spectrum of **1** were missing in the spectrum of **2**, which indicated that the isoprenyl moiety was absent in **2**. Analysis of the 2D NMR spectra (see Table S2 in Supporting Information) confirmed this conclusion. The third compound, stictamide C (**3**), was present only in a quantity sufficient for characterization by ^{1}H NMR and HRMS spectrometry. These data suggested that **3** was a methoxy derivative of **1**, based on the 14 amu difference in mass, while the chemical shift of this methoxy group noted in the ^{1}H NMR spectrum suggested a methyl ester rather than a phenolic ether. This conclusion was supported by a comparison of the ^{1}H NMR spectrum (Figure S11) with that of the trimethyl derivative **4**, prepared above, for which the methyl ester could be ascribed to the singlet at δ_H 3.64 through HMBC correlations. Additional support for this assignment was obtained from a comparison of the MS fragmentation patterns of **1** and **3** (Figure 3). Key fragmentations that established the position of methylation included a common m/z 536 ion derived from a retro-aldol fragmentation of the Ahppa unit and a y_1^+ ion in **1** that was shifted from m/z 182.3 by 14 amu to m/z 196.1 in **3**. Taken together, these fragments indicated that the C-terminal tyrosine had been methylated in **3**. Finally, identification of an ion at m/z 147.0 corresponding to $[y_1\text{-}NH_3\text{-}CH_3OH]^+$ conclusively established the methyl ester due to its loss of MeOH, which is typical of this functional group.

dx.doi.org/10.1021/jo200241h |*J. Org. Chem.* 2011, 76, 3635–3643

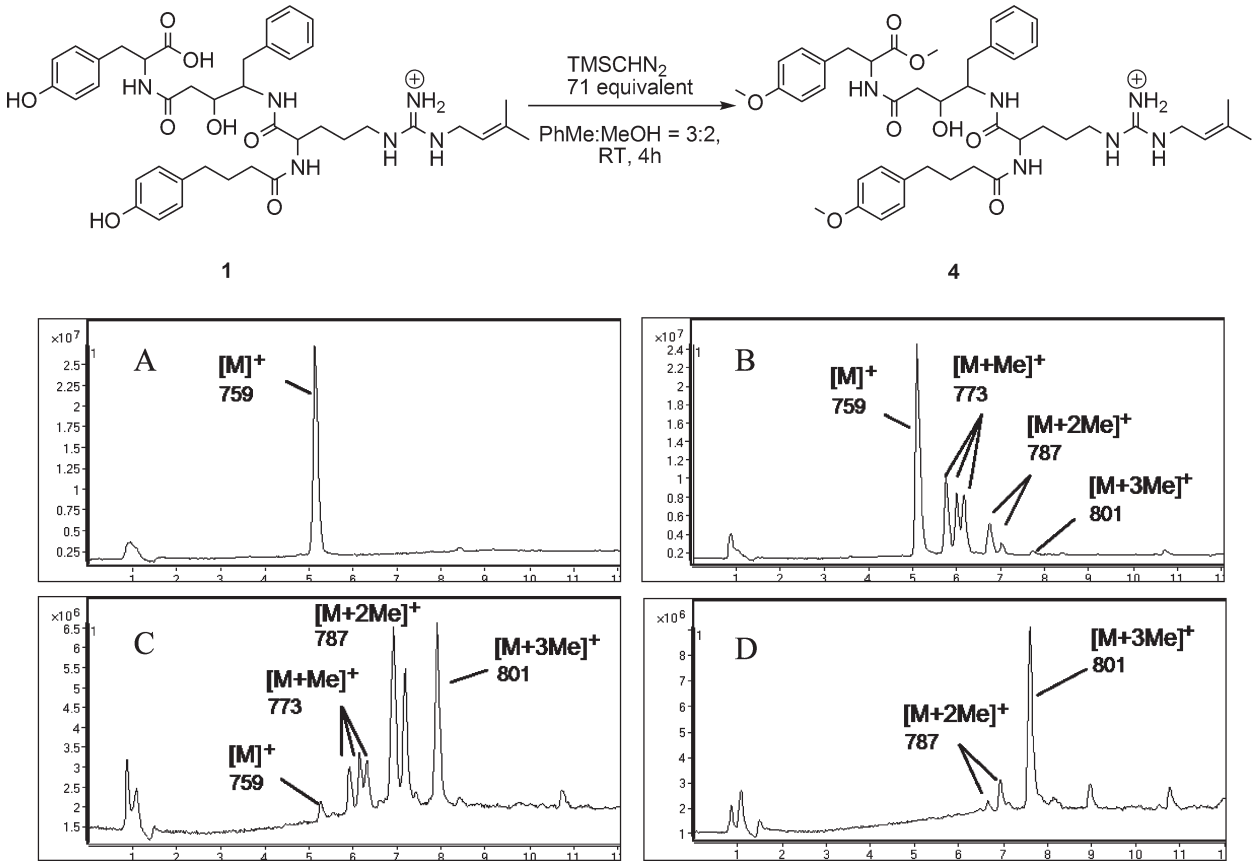

Figure 2. Methylation of **1** to distinguish a possible C-terminal carboxylic acid from a primary amide. LC-MS chromatogram of (A) starting material, (B) 15 min time point, (C) 1 h time point, and (D) 3.5 h time point.

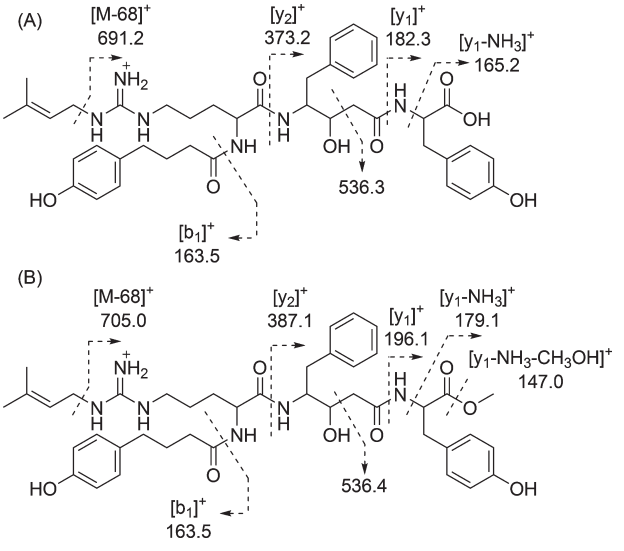

Figure 3. MS fragmentation patterns of (A) **1** and (B) **3**.

Methoxyaryl units, in contrast, tend to extrude carbon monoxide, which was not observed.

To determine the absolute configurations of the amino acid constituents, the advanced Marfey method was applied to **2**. The acid hydrolysate (0.5 mg, 6 N HCl, 118 °C, 10 h) of **2** was divided in two portions and derivatized with L- and DL-mixtures of (1-fluoro-2,4-dinitrophenyl)-5-leucinamide (FDLA)[7] as per

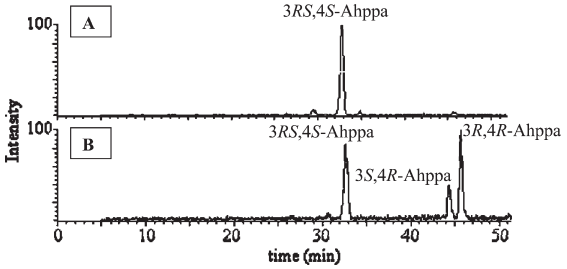

Figure 4. (A) L-FDLA and (B) DL-FDLA Ahppa extract-ion chromatograms of the derivatized hydrolysate of **2**.

the advanced Marfey's technique.[8] These experiments established that **2** contained D-Arg and L-Tyr. The identification of the latter was complicated by the predominance of *O*-aryl tyrosine products, where the diastereomeric derivatives were poorly resolved. The expected *N*-aryl tyrosine derivatives were eventually detected by extract-ion analysis of the LC-MS chromatograms and then confirmed through comparison with retention times and molecular weights of the appropriate standards.

Assigning the configuration of the vicinal centers in the Ahppa moiety via Marfey's analysis proved more challenging for multiple reasons. Initial experiments with synthetic standards[9] demonstrated that, while Marfey's derivatives could be prepared, distinguishing the 3*S*,4*S* and 3*R*,4*S* epimeric derivatives would be difficult under the standard solvent systems due to near identical retention times. Repeated attempts to optimize this

dx.doi.org/10.1021/jo200241h |*J. Org. Chem.* 2011, 76, 3635–3643

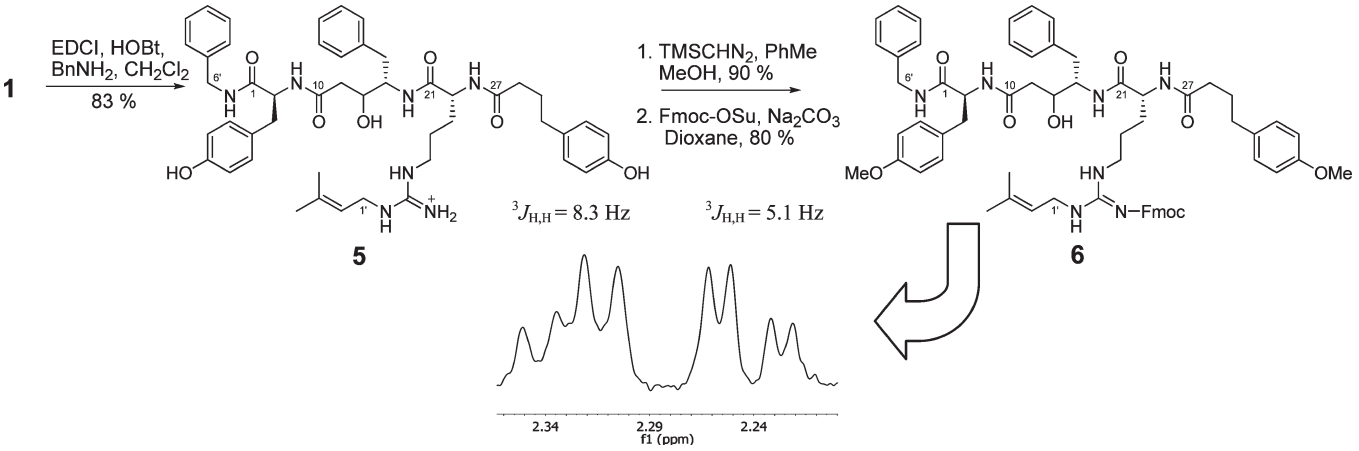

Figure 5. Preparation of the chloroform-soluble derivative **6** and its $^3J_{H,H}$ values used to establish the configuration of the intact Ahppa unit.

separation by varying the gradient or pH failed to resolve these standards. Unfortunately, analysis of the derivatized L-FDLA hydrolysate indicated that **2** contained one of these unresolved diastereomers (Figure 4A). While this established the 4*S* configuration, the relative stereochemistry still needed to be deduced. In the end, this was accomplished by "racemization" of the hydrolysate through derivatization with DL-FDLA and analyzing for D-FDLA-3*S*,4*S*- and D-FDLA-3*R*,4*S*-Ahppa. This analysis revealed that peaks corresponding to both C-3 epimers were present in the hydrolysate, although the 3*S*,4*S* diastereomer predominated by a ratio of approximately 2:1. Clearly, C-3, the β-alcohol of the Ahppa unit, undergoes epimerization at this center under the hydrolysis conditions. A similar phenomenon was noted by Sakai and Rinehart[10] during the structural characterization of the isostatine unit contained in didemnin B, which necessitated synthesis of that compound to clarify the issue. In our case, assuming the ratio of products in the hydrolysate does not simply represent a thermodynamic mixture, the configuration of the Ahppa unit therefore would be 3*S*,4*S*.

Although the preceding results established the stereochemistry of the hydrolyzed Ahppa unit, they did not conclusively establish the stereochemistry of this unit in the natural product due to the possibility of inversion at C-3 during hydrolysis. We recently proposed a simple method to assign the relative configuration of statine derivatives (5-alkyl-4-amino-3-hydroxybutanoic acids) to address this question.[9] This method allows configurational assignment of statine-type units within complex natural products without degradation, as the *syn* and *anti* diastereomers can be distinguished using a combination of chemical shift and coupling constant information derived from the α-methylene ABX system. The method was validated using 73 examples, ranging in structural complexity from simple statine-type units to cyclic depsipeptides, such as tamandarin B,[11] demonstrating the scope and limitations of the methodology.

One of the principle limitations of the method is the requirement for $CDCl_3$ solubility, presumably to facilitate hydrogen bonding between the various heteroatoms in this unit. As compounds **1**−**3** are insoluble in $CDCl_3$, we sought to prepare a more lipophilic derivative. Treatment of **1** with an excess of trimethylsilyldiazomethane,[12] as described above, yielded **4**, but subsequent derivatization with Fmoc-OSu failed to provide the desired derivative. While the methylation proceeded smoothly, the derivatization of the guanidino amine was so slow that hydrolysis of the methyl ester competed, under a variety of conditions, to yield a mixture of products. Given this liability, compound **1** was therefore converted to the secondary amide **5** through coupling with benzylamine, and then the phenolic groups were methylated (Figure 5). Treatment of this derivative with Fmoc-OSu cleanly afforded the desired product **6** without competing hydrolysis. Careful analysis of the proton spectrum of this derivative, **6**, recorded in $CDCl_3$, revealed the correct diagnostic pattern for the methylene protons of the ABX system of the Ahppa unit. In this case, the downfield methylene proton resonating at δ_H 2.33 was a doublet of doublets with a large vicinal $^3J_{H,H}$ value of 8.3 Hz, while the upfield signal (δ_H 2.24) had the small vicinal proton coupling (5.1 Hz). These results confirmed the *anti* stereochemical configuration of the Ahppa unit.

The Ahppa unit has been found in a rather limited number of compounds. It is a component of the cyanobacterial metabolites, tasiamide B[13] and hapalosin,[4] and of some protease inhibitors isolated from *Streptomyces* spp.[14] The stictamides represent the first reported example of this structural motif in a lichen secondary metabolite.

Given the presence of a γ-amino-β-hydroxy acid moiety in **1**, which is a common design element in protease inhibitors, stictamide A (**1**) was evaluated for selectivity against a series of 18 proteases (Table 2). Compound **1** did not inhibit the serine proteases trypsin, chymotrypsin, or elastase in standard chemiluminescent assays at concentrations up to 100 μM.[15] It was inactive (IC_{50} >100 μM) against the Alzheimer's relevant proteases BACE1 (β-secretase), ADAM10 (α-secretase), and TACE (potential γ-secretase) and against angiotensin converting enzyme 1 (ACE1), caspase 3, ADAM9, and calpain. Compound **1** did inhibit matrix metalloproteinase-12 (MMP12) with an IC_{50} value of 2.3 μM (K_i = 4.9 μM), while related MMPs (2 and 9) were inhibited only at significantly higher concentrations (37 and 65 μM).

Matrix metalloproteinases (MMPs) are zinc-dependent endopeptidases that mediate extracellular matrix degradation and thereby are involved in many physiological and pathological processes including angiogenesis and tumor invasion. That MMPs are required to initiate tumor cell invasion into the surrounding matrix has been the underlying principle in the study of cancer cell invasion for a number of years.[16] Despite

Table 1. NMR Spectroscopic Data for Stictamide A (1) at 500 MHz in MeOH-d_4

residue	position	δ_C, mult.	δ_H (J in Hz)	COSY	HMBC	TOCSY[a]
Tyr	1	178.9, qC			H-2, H-3a, H-3b	
	2	57.8, CH	4.44, dd (8.5, 4.3)		H-3a, H-3b	H-3a, H-3b, NH(1) [a]
	3	38.2, CH_2	3.13, dd (14.0, 4.3)	H-2	H-2, H-5	
			2.86, dd (14.0, 8.5)			
	4	130.5, qC			H-2, H-6	
	5 and 9	131.4, CH	7.06, d (8.5)	H-6	H-3a, H-3b	
	6 and 8	116.0, CH	6.66, d (8.5)			
	7	156.9, qC			H-5, H-6	
Ahppa	10	172.5, qC			H-2, H-11a, H-11b, H-12	
	11	41.4, CH_2	2.39, dd (14.1, 7.0)	H-12	H-12	
			2.29, dd (14.1, 6.8)	H-12		
	12	70.1, CH	4.08, m		H-11a, H-11b, H-14b	H-11a, H-11b, H-13, H-14a, H-14b
	13	56.8, CH	4.10, m		H-11a, H-11b, H-14a, H-14b	H-11a, H-11b, H-12, H-14a, H-14b
	14	36.7, CH_2	2.95, dd (13.7, 4.5)	H-13	H-16	
			2.84, dd (13.7, 10.5)	H-13		
	15	140.1, qC			H-14a, H-14b, H-17	
	16 and 20	130.4, CH	7.22, d (7.4)	H-17	H-14a, H-14b, H-18	
	17 and 19	129.3, CH	7.19, t (7.4)			
	18	127.2, CH	7.11, t (7.4)	H-17	H-16	
Arg	21	174.3, qC			H-13, H-22	
	22	54.5, CH	4.19, dd (7.6, 6.2)		H-23a	H-23a, H-23b, H-24a, H-24b, H-25
	23	30.2, CH_2	1.60, m	H-22, H-24	H-22, H-24b, H-25	
			1.42, m			
	24	26.1, CH_2	1.40, m	H-25	H-22, H-23a, H-25	
			1.31, m			
	25	41.9, CH_2	3.07, t (5.9)			
	26	157.3, qC			H-25, H-1′	
N-prenyl	1′	40.5, CH_2	3.76, d (7.1)	H-2′, H-4′, H-5′	H-2′	
	2′	119.6, CH	5.24, t (7.1)		H-1′, H-4′, H-5′	H-1′, H-4′, H-5′
	3′	138.7, qC			H-1′, H-4′, H-5′	
	4′	25.8, CH_3	1.74, s	H-2′	H-2′, H-5′	
	5′	18.0, CH_3	1.69, s	H-2′	H-2′, H-4′	
HO-Ph-Bu	27	175.9, qC			H-22, H-28, H-29	
	28	36.4, CH_2	2.23, t (7.6)		H-29, H-30	
	29	29.0, CH_2	1.83, p (7.6)	H-28, H-30	H-28, H-30	
	30	35.5, CH_2	2.52, t (7.6)		H-28, H-29, H-32	H-28, H-29
	31	133.8, qC			H-29, H-30, H-33	
	32 and 36	130.4, CH	6.99, d (8.4)	H-33	H-30	
	33 and 35	116.1, CH	6.68, d (8.4)		H-32	
	34	156.5, qC			H-32, H-33	
NH(1)[a]			7.75, d (8.1)			

[a] Protons observed in MeOH-d_3.

significant research, the timing of this process, how it is regulated in the tumor microenvironment, and how it varies with cell type still remain major unanswered questions in cancer biology.[17] The lack of more detailed mechanisms of action for the full range of MMPs in the tumor microenvironment, and of the other physiological roles of MMPs, undoubtedly contributed to the lack of efficacy observed in the clinical trials of broad spectrum MMP inhibitors.[18] In the past few years, there has been a resurgence of interest in these targets as they have been discovered to modulate a diverse array of biochemical processes in cancer, including growth signals, tumor angiogenesis, apoptosis, neoplastic progression, invasion, and metastasis.[17] In particular, MMP12, secreted macrophage metalloelastase, has recently been shown to promote glioma invasion and to be upregulated in gliomas by the matrix glycoprotein tenascin C.[19] It is also proinflammatory, as MMP12 overexpression has been implicated in emphysema,[20] osteoarthritis,[21] atherosclerosis,[22] and chronic obstructive pulmonary disease.[23]

Matrix metalloproteinases have attracted considerable interest as targets for antiangiogenic agents, although it is now recognized that isozyme selective inhibitors are needed to exploit these targets effectively.[17] Inhibitors of MMP2 and MMP9, based primarily on hydroxamate zinc-binding motifs, were evaluated in clinical trials, although none displayed the requisite safety and

dx.doi.org/10.1021/jo200241h |*J. Org. Chem.* 2011, 76, 3635–3643

Table 2. Protease Screening of 1

target protease	IC_{50} (μM)	inactive
MMP12	2.3	ADAM9
cathepsin E	11	ADAM10
cathepsin D	20	ACE1
DDP IV	26	calpain
MMP2	37	caspase 3
cathepsin B	49	TACE
MMP9	65	trypsin
caspase 9	84	chymotrypsin
		elastase
		BACE1

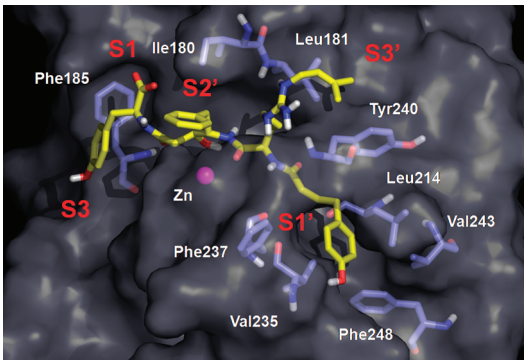

Figure 6. Docked structure of **1** with MMP12.

efficacy profiles required for phase III approval,[18] which suggests a more complex interplay of factors than previously realized. Carboxylate inhibitors of MMPs have also been reported that bind to the zinc ion,[24] which, given the presence of this functionality in **1**, suggested a possible mechanism by which **1** was inhibiting MMP12.

The interaction of **1** with MMP12 was further examined by docking with AutoDock Vina 1.1.1,[25] using the X-ray structure of MMP12 (PDB code 1RMZ).[26] Water molecules within the crystal structure were removed, while hydrogens attached to electronegative atoms and Gasteiger charges were added using AutoDockTools. Optimized zinc parameters were applied to improve the accuracy of the docking.[27] Ligands, which were optimized for their energy and geometry using MM2 and AM1 force fields, were docked into this protein structure. Using these parameters, ligand NNGH was successfully docked into MMP12, with a rmsd of 0.84 Å compared to its original crystal structure. Stictamide A (**1**) was then docked as the carboxylate and the guanidinium zwitterion to reflect a physiologically relevant state (Figure 6). These results suggest that **1** and MMP12 interact via a non-zinc-binding mode, rather than the more common carboxylate−zinc interaction. Non-zinc-binding inhibitors of MMP12 have been previously reported that exploit the deep hydrophobic S1′ pocket for both potency and selectivity, including those with carboxylate termini.[28] In the case of **1**, the 4-(4-hydroxyphenyl)butanoic acid residue is situated within this critical pocket potentially stabilized by interactions with Phe237, Phe248, and Val 235. Given the low homology of S1′ pockets in MMPs, optimizing interactions within this unit will be crucial for improving selectivity and potency.[29−31]

As noted above, **1** inhibited several proteases that can affect the tumor microenvironment leading to changes in inflammation, angiogenesis, cancer cell growth, cell death, and cell invasion.[32,33] In particular, MMP2, MMP12, cathepsin B, and cathepsin D are known to contribute to glioma cell invasion.[32−37] As such, we examined the effect of **1** on invasion of a glioblastoma derived cell line (U87-MG) through a three-dimensional extracellular matrix (Matrigel) in an in vitro transwell assay. At a concentration of 5 μM, cell invasion was significantly affected in the treated cells (Figure 7B). To exclude any possible cytotoxic effects of **1** on U87-MG cells, we examined cell viability after incubation with 5 μM (Figure 7A) or 50 μM (data not shown) of stictamide A. Compared to control samples that were incubated with the DMSO vehicle, **1** did not significantly alter U87-MG viability at either concentration (Figure 7A). Therefore, at a concentration that predominantly impairs MMP12 function in enzymatic systems, **1** significantly reduces invasion of U87-MG cells in vitro.

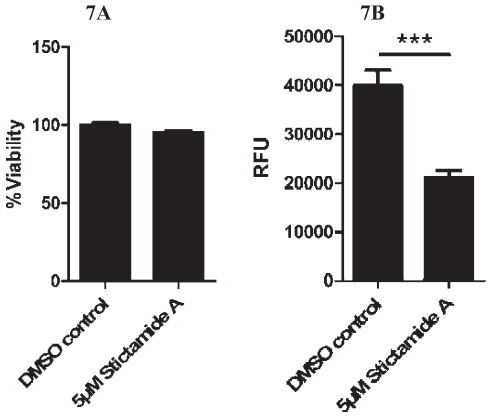

Figure 7. Effects of stictamide A (**1**) on U78-MG cells after 20 h. (A) Cell viability (5 μM). (B) Cell invasion (5 μM). The fluorescence emission (RFU) is proportional to the number of invasive cells. Error bars indicate the standard error of the mean.

EXPERIMENTAL PROCEDURES

Collection and Identification. The sample designated 122899-SOLE-5 was collected on the river banks of "RIO SOLE" in the community of Guaca, near David City, Chiriqui, Panama, on December 28, 1999. A NCBI BLAST analysis of the ITS sequence of this strain showed the highest identity to the lichen genus *Sticta*. The multiple sequences available for this genus on Genbank were downloaded and aligned in MEGA 4. A sequence of the closely related genus *Lobaria* (*Lobaria linita* AB239702) was also included. Ambiguous parts of the alignment were trimmed, leaving 388 bp for sequence clustering using neighbor joining (maximum likelihood composite model with a 1000 bootstrap and pairwise deletion option). Branch support >70% is not displayed on the resulting tree. The labels for the polyphyletic species were also not included for tree clarity, as they represent taxonomic discrepancies between researchers.

The analysis demonstrated that the *Sticta* species investigated lay on a long branch and was well separated from other members of the genus that have been characterized using molecular methods to date. A voucher specimen has been stored at the UH Manoa, Department of Chemistry, and is available upon request. Sequences obtained from the specimen have been deposited in GenBank under accession numbers HQ149042−HQ149045.

Extraction and Isolation. A portion of the freeze-dried sample was exhaustively extracted with MTBE/MeOH (2:8) to yield 9.6 g of crude extract, which after trituration with MeOH afforded 3.7 g of a

desalted extract. This mixture was separated on a C_8 flash column (25 g) eluting with a step gradient of 25, 50, 75, and 100% MeOH (×2) in H_2O to provide five fractions (A−E) of 2.8 g, 87 mg, 78 mg, 203 mg, and 33 mg, respectively. LC-MS analyses of these fractions revealed that three of them contained a series of compounds with molecular weights between 600 and 800 amu. Separation of fraction C (78 mg) by reversed-phase HPLC [Onyx C_{18}, 100 × 10 mm, a linear gradient over 35 min from 5 to 100% MeCN in H_2O with 0.1% formic acid added to both solvents, flow rate 5 mL/min, PDA and ELSD detection] afforded stictamide A (**1**) (t_R 13.7 min, 2.5 mg). Separation of fraction B (87 mg) by RP-HPLC [Onyx C_{18}, 100 × 10 mm, a linear gradient over 15 min from 15 to 50 % MeCN in H_2O then 50 to 100% over 10 min with 0.1 % formic acid added to both solvents, flow rate 5 mL/min, PDA detection] afforded stictamide A (t_R 9.6 min, 2.0 mg, 0.047 % total yield) and stictamide B (**2**) (t_R 7.4 min, 3.1 mg, 0.032 % yield). Separation of fraction D (203 mg) using the same conditions as for fraction C reported above, yielded impure stictamide C (t_R 15.6 min), which was repurified by RP-HPLC [Luna C_8, 150 × 4.6 mm, a linear gradient from 5 to 50% aqueous MeCN with 0.1% formic acid in both solvents over 30 min, flow rate 0.7 mL/min, PDA] to yield stictamide C (**3**) (t_R 29.5 min, 0.2 mg, 0.002% yield).

*Stictamide A (**1**):* Light yellow amorphous powder; $[\alpha]^{22}_D$ −0.2 (*c* 0.2, MeOH), UV (MeOH) λ_{max} (log ε) 219 (8.9), 276 (6.8) nm; IR (CaF_2) ν_{max} 3399, 2924, 2856, 1629, 1449, 1383, 1260, 1088 cm^{-1}; see Table 1 for tabulated spectral data; HRESI-TOFMS *m*/*z* $[M]^+$ 759.4082 [calcd for $C_{41}H_{55}N_6O_8^+$, 759.4081, −0.1 ppm error].

*Stictamide B (**2**):* Light yellow amorphous powder; $[\alpha]^{22}_D$ −0.5 (*c* 0.2, MeOH); UV (MeOH) λ_{max} (log ε) 219 (9.3), 276 (7.5) nm; IR (CaF_2) ν_{max} 3275, 2830, 2361, 1591, 1514, 1362, 1245 cm^{-1}; see Table S2 in the Supporting Information for tabulated spectral data; HRESI-TOFMS *m*/*z* $[M]^+$ 691.3457 [calcd for $C_{36}H_{47}N_6O_8^+$, 691.3455, −0.2 ppm error].

*Stictamide C (**3**):* Light yellow amorphous powder; $[\alpha]^{22}_D$ 0.1 (*c* 0.2, MeOH); UV (MeOH) λ_{max} (log ε) 219 (7.5), 276 (6.4) nm; IR (CaF_2) ν_{max} 3404, 2951, 2925, 2853, 1628, 1454, 1385, 1353, 1318, 1088 cm^{-1}; ^{1}H NMR (500 MHz, MeOH-d_4) δ_H 1.31−1.60 (m, 4H, H-23a, H-23b, H-24a, H-24b), 1.70 (s, 3H, H-5′), 1.75 (s, 3H, H-4′), 1.84 (p, *J* = 7.3 Hz, 2H, H-29), 2.15 (t, *J* = 7.3 Hz, 2H, H-28), 2.23 (dd, *J* = 14.0, 7.0 Hz, 1H, H-11b), 2.35 (dd, *J* = 14.0, 7.0 Hz, 1H, H-11a), 2.51 (t, *J* = 7.3 Hz, 2H, H-30), 2.87 (dd, *J* = 13.9, 9.0 Hz, 1H, H-14b), 2.92 (dd, *J* = 14.3, 6.5 Hz, 1H, H-3b), 2.99 (dd, *J* = 13.9, 5.7 Hz, 1H, H-14a), 3.04 (br, 2H, H-25), 3.18 (dd, *J* = 14.3, 4.6 Hz, 1H, H-3a), 3.64 (s, 3H, H-6′), 3.77 (d, *J* = 6.2 Hz, 2H, H-1′), 4.00 (dt, *J* = 7.0, 1.5 Hz, 1H, H-12), 4.19 (dd, *J* = 6.0, 4.8 Hz, 1H, H-22), 4.24 (ddd, *J* = 9.0, 5.7, 1.5 Hz, 1H, H-13), 4.54 (dd, *J* = 6.5, 4.6 Hz, 1H, H-2), 5.25 (t, *J* = 6.2 Hz, 1H, H-2′), 6.67 (d, *J* = 8.1 Hz, 2H, H-6, H-8), 6.69 (d, *J* = 7.8 Hz, 2H, H-33, H-35), 6.97 (d, *J* = 7.8 Hz, 2H, H-32, H-36), 7.00 (d, *J* = 8.1 Hz, 2H, H-5, H-9), 7.14 (m, 1H, H-18), 7.22 (m, 2H, H-17, H-19), 7.24 (m, 2H, H-16, H-20); HRESI-TOFMS *m*/*z* $[M]^+$ 773.4243 [calcd for $C_{42}H_{57}N_6O_8^+$, 773.4238, −0.6 ppm error].

*Trimethyl Stictamide A (**4**).* A 150 μL aliquot of 0.2 M $TMSCHN_2$ in toluene (30 μmol) was added to a solution of 0.5 mg of **1** (0.7 μmol) in 100 μL of methanol. After stirring for 3 h at room temperature, another 100 μL of 0.2 M $TMSCHN_2$ (20 μmol) was added and the solution stirred for an additional 1 h before the solvent was removed under a vacuum to afford the crude reaction mixture. The final product was purified by RP-HPLC [Luna C_8, 150 × 4.6 mm, a linear gradient over 40 min using 20−80% aqueous MeCN with 0.1% formic acid in both solvents, flow rate 0.7 mL/min, PDA detection] to afford **4** (t_R 19.5 min, 0.4 mg, 76% yield). **4**: Light yellow amorphous powder; $[\alpha]^{22}_D$ −0.4 (*c* 0.2, MeOH); UV (MeOH) λ_{max} (log ε) 225 (7.9), 276 (6.1) nm; IR (CaF_2) ν_{max} 3442, 2957, 2926, 2851, 1638, 1596, 1513, 1450, 1385, 1353, 1319, 1247, 1085 cm^{-1}; see Table S3 in the Supporting Information for tabulated spectral data; HRESI-TOFMS *m*/*z* $[M]^+$ 801.4547 [calcd for $C_{44}H_{61}N_6O_8^+$, 801.4551, 0.5 ppm error].

*Benzylamidation of **1** (**5**).* A sample containing 2 mg of EDCI (13 μmol), 2 mg of HOBt (15 μmol), and 1.4 mg of **1** (1.9 μmol) was dissolved in 500 μL of CH_2Cl_2 and cooled in an ice bath under a N_2 atmosphere. To this solution was added 10 μL of benzylamine (90 μmol). A second and third aliquot of EDCI (32 μmol each time) were added on days 2 and 3, while the reaction stirred at room temperature. The reaction was quenched after a total of 7 days by the addition of 1 N HCl and residue partitioned between H_2O and EtOAc. The final product was purified from the organic residue by RP-HPLC [Luna C_8, 150 × 4.6 mm, a linear gradient over 40 min using 20−80% aqueous MeCN with 0.1% formic acid in both solvents, flow rate 0.7 mL/min, PDA detection] to afford 1.3 mg of **5** (83% yield). **5**: Light yellow amorphous powder; $[\alpha]^{22}_D$ 0.4 (*c* 0.2, MeOH); UV (MeOH) λ_{max} (log ε) 225 (7.4), 278 (5.7) nm; IR (CaF_2) ν_{max} 3395, 2965, 2931, 2820, 1639, 1593, 1515, 1454, 1385, 1353, 1085 cm^{-1}; ^{1}H NMR (500 MHz, MeOH-d_4) δ_H 1.30 (m, 1H, H-24b), 1.35 (m, 1H, H-24a), 1.45 (m, 1H, H-23b), 1.60 (m, 1H, H-23a), 1.70 (s, 3H, H-5′), 1.75 (s, 3H, H-4′), 1.83 (p, *J* = 7.6 Hz, 2H, H-29), 2.18 (t, *J* = 7.6 Hz, 2H, H-28), 2.32 (dd, *J* = 14.4, 7.2 Hz, 1H, H-11b), 2.40 (dd, *J* = 14.4, 7.2 Hz, 1H, H-11a), 2.48 (t, *J* = 7.6 Hz, 2H, H-30), 2.77 (dd, *J* = 13.0, 6.7 Hz, 1H, H-14b), 2.79 (m, 1H, H-3b), 2.86 (dd, *J* = 13.0, 5.5 Hz, 1H, H-14a), 2.96 (m, 2H, H-25), 3.02 (m, 1H, H-3a), 3.76 (d, *J* = 6.8 Hz, 2H, H-1′), 4.05 (td, *J* = 7.2, 1.4 Hz, 1H, H-12), 4.09 (m, 1H, H-22), 4.11 (m, 1H, H-13), 4.32 (d, *J* = 4.6 Hz, 2H, H-6′), 4.47 (dd, *J* = 8.2, 5.9 Hz, 1H, H-2), 5.24 (t, *J* = 6.8 Hz, 1H, H-2′), 6.58 (d, *J* = 8.3 Hz, 2H, H-6, H-8), 6.59 (d, *J* = 8.3 Hz, 2H, H-33, H-35), 6.87 (d, *J* = 8.3 Hz, 2H, H-32, H-36), 6.92 (d, *J* = 8.3 Hz, 2H, H-5, H-9), 7.11 (m, 1H, H-18), 7.12 (m, 2H, H-16, H-20), 7.17 (m, 3H, H-17, H-19, H-10′), 7.18 (m, 2H, H-8′, H-12′), 7.26 (t, *J* = 7.4 Hz, 2H, H-9′, H-11′); HRESI-TOFMS *m*/*z* $[M]^+$ 848.4704 [calcd for $C_{48}H_{62}N_7O_7^+$, 848.4711, 0.8 ppm error].

*Methylation and Fmoc Protection (**6**).* A 300 μL aliquot of 0.4 M $TMSCHN_2$ in toluene (120 μmol) was added to a solution of 1.3 mg of **5** (1.5 μmol) dissolved in 200 μL of methanol. After stirring for 4 h at room temperature, the solvent was removed and the crude reaction mixture was purified by RP-HPLC [Luna C_8, 150 × 4.6 mm, a linear gradient over 40 min using 20−80% aqueous MeCN with 0.1% formic acid in both solvents, flow rate 0.7 mL/min, PDA detection] to afford the dimethyl product in 90% yield (1.2 mg). This product (1.4 μmol) was dissolved in 9% Na_2CO_3 (150 μL) and dioxane (150 μL). After stirring in an ice bath for 15 min, 50 μL of a 0.28 M solution of Fmoc-OSu (14 μmol) was added to the reactants and the mixture was stirred at 0 °C for an additional 30 min before warming to room temperature. Two additional aliquots of 0.28 M Fmoc-OSu (each 14 μmol in 50 μL) were added on days 2 and 4. On day 6, the solvent was removed *in vacuo* and then the residue was partitioned between EtOAc and H_2O. The organic residue was purified by RP-HPLC [Luna C_8, 150 × 4.6 mm, a linear gradient over 40 min using 20−80% aqueous MeCN with 0.1% formic acid in both solvents, flow rate 0.7 mL/min, PDA detection] to afford **6** (1.2 mg, 80% yield). **6**: White amorphous powder; $[\alpha]^{22}_D$ 0.5 (*c* 0.2, MeOH); UV (MeOH) λ_{max} (log ε) 219 (8.8), 228 (8.6), 265 (7.8), 300 (4.3) nm; IR (CaF_2) ν_{max} 3440, 2952, 2923, 2852, 1593, 1513, 1450, 1383, 1352, 1318, 1247, 1085 cm^{-1}; see Table S4 in the Supporting Information for tabulated spectral data; HRESI-TOFMS *m*/*z* $[M + H]^+$ 1098.5667 [calcd for $C_{65}H_{76}N_7O_9^+$, 1098.5705, 3.5 ppm error], *m*/*z* $[M + Na]^+$ 1120.5503 [calcd for $C_{65}H_{75}N_7O_9Na^+$, 1120.5524, 1.9 ppm error].

Advanced Marfey Analysis. A 500 μg sample of **2** was hydrolyzed at 118 °C for 10 h with 200 μL of 6 N HCl. The hydrolysate was passed over a small C_8 column and the resulting eluant divided into two portions before drying. Each portion was derivatized by adding 100 μL of H_2O, 50 μL of 1 M sodium bicarbonate, and 50 μL of 6 mg/mL of either L- or DL-FDLA in acetone. After stirring for 3 min at 81 °C, the reaction was quenched by the addition of 50 μL of 1 N HCl and then diluted with 150 μL of acetonitrile. The resulting L- and DL-FDLA

derivatives were analyzed by ESI-LCMS-TOF [Luna C_8, 150 × 4.6 mm, a linear gradient with 30−50% aqueous MeCN with 0.01% TFA in both solvents over 50 min, flow rate 0.7 mL/min], and the retention times were compared with those of standards. The retention times of the DL-FDLA-derivatized (3*S*,4*S*)-Ahppa standards were 32.6 and 45.7 min, while the retention times of the DL-FDLA-derivatized (3*R*,4*S*)-Ahppa standards were 32.2 and 44.2 min. The retention times of the L-FDLA-derivatized amino acids from the hydrolysate were D-Arg (11.3 min), L-Tyr (27.1 min), and (3*S*,4*S*)-Ahppa (32.4 min). The retention times of the D-FDLA-derivatized amino acids from the DL-FDLA-derivatized hydrolysate were D-Arg (14.4 min), L-Tyr (30.1 min), and (3*S*,4*S*)-Ahppa (45.7 min).

Cell Invasion Assay. ThinCert tissue culture inserts (8.0 μm pore size) were coated overnight at 4 °C with 10 μg/mL human plasma fibronectin. The inside of the cell culture inserts was then coated with Matrigel Basement Membrane Matrix (growth factor reduced) according to the manufacturer's protocol. The matrix was supplemented with 5 or 50 μM of **1** or DMSO control. On the day of the assay, U87-MG cells were trypsinized and a total of 1 million cells were plated on the coated tissue culture inserts in D-MEM that had been supplemented with non-essential amino acids. Inserts were placed in the wells of a 24-well plate filled with D-MEM supplemented with non-essential amino acids and 10 ng/mL EGF. Cells were incubated for 20 h at 37 °C, 5% CO_2. Cell culture medium was then removed from the wells, replaced with D-MEM containing 8 μM calcein-AM, and incubated for 45 min at 37 °C under 5% CO_2. Then, the culture medium was removed from the tissue culture inserts, and the inserts were transferred to a freshly prepared well containing 0.05% trypsin-EDTA. After a 10 min incubation at 37 °C under 5% CO_2 with sporadic agitation, the inserts were discarded. The trypsin-EDTA solution then contained the detached invasive cells. Invasion was quantified by measuring the fluorescence emission of calcein-AM at 520 nm upon excitation at 485 nm in black 96-well plates with a fluorescence plate reader. Experiments were done in duplicate, and fluorescence emissions were measured in triplicate. All data are shown as mean plus standard error of the mean (SEM). Statistical significance was calculated using the Student's *t* test. The *p* values of <0.05 were considered to be statistically significant.

Cell Viability Assay. U87-MG cells (10^4 per well) were incubated with **1** at a concentration of 5 or 50 μM in a 96-well plate. Control samples were incubated with the carrier DMSO in an equivalent volume. After an incubation time of 20 h, cell viability was measured using the alamarBlue cell viability reagent according to the manufacturer's protocol. Cell viability was determined by measuring the fluorescence emission intensity at 590 nm upon excitation at 560 nm with a fluorescence plate reader. Samples were prepared in quintuplicate, but the experiment was repeated once. All data are shown as mean plus standard error of the mean (SEM). Statistical significance was calculated using the Student's *t* test. The *p* values of <0.05 were considered to be statistically significant.

Molecular Docking. Compound **1** was docked with MMP12 using the X-ray structure of MMP12 (PDB code 1RMZ)[26] and AutoDock Vina 1.1.1.[25] Water molecules within the crystal structure were removed and polar hydrogens and Gasteiger charges were added using AutoDockTools. Optimized zinc parameters were applied to improve docking accuracy.[27] Ligands were optimized for their energy and geometry using MM2 and AM1 force fields before docking. In the structures of the ligands, all bonds were treated as rotatable except for the aromatic, alkenyl, amide, and guanidino bonds. Stictamide A (**1**) was docked as the carboxylate and the guanidinium zwitterion to reflect a physiologically relevant state. The dimensions of the grid map were 26 × 24 × 26 points with a grid-point spacing of 1 Å. The center of the grid was set to coincide with the catalytic zinc atom. Docking proceeded with an exhaustiveness value of 600 and a maximum output of 100 structures.

■ ASSOCIATED CONTENT

Supporting Information. Tabulated NMR data for **1**, **2**, **4**, and **6** along with ^{1}H, ^{13}C, gCOSY, gHMBC, and gHSQC NMR spectra for **1**, **2**, and **6**; ^{1}H and gHMBC spectra for **4** and **5**, and ESI-LC-MS-TOF chromatograms of amino acid FDLA derivatives. This material is available free of charge via the Internet at http://pubs.acs.org.

■ AUTHOR INFORMATION

Corresponding Author
*Phone: 808-956-5720. Fax: 808-956-5908. E-mail: philipwi@hawaii.edu.

■ ACKNOWLEDGMENT

This work was funded by grants from the Alzheimer's Association (NIRG-08-90880), Victoria S. and Bradley L. Geist Foundation, the Alzheimer's Drug Discovery Foundation (281204), the National Institute of Aging (1R21AG032405), and NIGMS (R01GM088266 to J.R.). Funds for the upgrades of the NMR instrumentation were provided by the CRIF program of the National Science Foundation (CH E9974921) and the Elsa Pardee Foundation. The purchase of the Agilent LC-MS was funded by Grant W911NF-04-1-0344 from the Department of Defense. We thank A. Preciado for the phenylalanine-statine standards, F.D. Horgen and T. Vansach for help with acquisition of the LC-MS spectra, and B. Rubio for the serine protease data.

■ REFERENCES

(1) Morishima, H.; Takita, T.; Aoyagi, T.; Takeuchi, T.; Umezawa, H. *J. Antibiot.* **1970**, *25*, 263–265.
(2) Morishima, H.; Sawa, T.; Takita, T.; Aoyagi, T.; Takeuchi, T.; Umezawa, H. *J. Antibiot.* **1974**, *27*, 267–273.
(3) Rinehart, K.; Gloer, J.; Hughes, R.; Renis, H.; McGovren, J.; Swynenberg, E.; Stringfellow, D.; Kuentzel, S.; Li, L. *Science* **1981**, *212*, 933–935.
(4) Stratmann, K.; Burgoyne, D. L.; Moore, R. E.; Patterson, G. M. L.; Smith, C. D. *J. Org. Chem.* **1994**, *59*, 7219–7226.
(5) Marciniszyn, J.; Hartsuck, J. A.; Tang, J. *J. Biol. Chem.* **1976**, *251*, 7088–7094.
(6) Fehrentz, J. A.; Chomier, B.; Bignon, E.; Venaud, S.; Chermann, J. C.; Nisato, D. *Biochem. Biophys. Res. Commun.* **1992**, *188*, 865–872.
(7) Marfey, P. *Carlsberg Res. Commun.* **1984**, *49*, 591–596.
(8) Fujii, K.; Ikai, Y.; Oka, H.; Suzuki, M.; Harada, K.-I. *Anal. Chem.* **1997**, *69*, 5146–5151.
(9) Preciado, A.; Williams, P. G. *J. Org. Chem.* **2008**, *73*, 9228–9234.
(10) Rinehart, K. L.; Sakai, R.; Kishore, V.; Sullins, D. W.; Li, K. M. *J. Org. Chem.* **1992**, *57*, 3007–3013.
(11) Vervoort, H.; Fenical, W.; Epifanio, R. de A. *J. Org. Chem.* **2000**, *65*, 782–792.
(12) Kühnel, E.; Laffan, D. D. P.; Lloyd-Jones, G. C.; Martínez del Campo, T.; Shepperson, I. R.; Slaughter, J. L. *Angew. Chem., Int. Ed.* **2007**, *46*, 7075–7078.
(13) Williams, P. G.; Yoshida, W. Y.; Moore, R. E.; Paul, V. J. *J. Nat. Prod.* **2003**, *66*, 1006–1009.
(14) Sato, T.; Shibazaki, M.; Yamaguchi, H.; Abe, K. *J. Antibiot.* **1994**, *47*, 588–590.
(15) Gunasekera, S. P.; Miller, M. W.; Kwan, J. C.; Luesch, H.; Paul, V. J. *J. Nat. Prod.* **2010**, *73*, 459–462.
(16) Liotta, L. A.; Tryggvason, K.; Garbisa, S.; Hart, I.; Foltz, C. M.; Shafie, S. *Nature* **1980**, *284*, 67–68.
(17) Kessenbrock, K.; Plaks, V.; Werb, Z. *Cell* **2010**, *141*, 52–67.

(18) Coussens, L. M.; Fingleton, B.; Matrisian, L. M. *Science* **2002**, *295*, 2387–2392.
(19) Sarkar, S.; Nuttall, R. K.; Liu, S.; Edwards, D. R.; Yong, V. W. *Cancer Res.* **2006**, *66*, 11771–11780.
(20) Houghton, A. M.; Quintero, P. A.; Perkins, D. L.; Kobayashi, D. K.; Kelley, D. G.; Marconcini, L. A.; Mecham, R. P.; Senior, R. M.; Shapiro, S. D. *J. Clin. Invest.* **2006**, *116*, 753–759.
(21) Liu, M.; Sun, H.; Wang, X.; Koike, T.; Mishima, H.; Ikeda, K.; Watanabe, T.; Ochiai, N.; Fan, J. *Arthritis Rheum.* **2004**, *50*, 3112–3117.
(22) Halpert, I.; Sires, U. I.; Roby, J. D.; Potter-Perigo, S.; Wight, T. N.; Shapiro, S. D.; Welgus, H. G.; Wickline, S. A.; Parks, W. C. *Proc. Natl. Acad. Sci. U.S.A.* **1996**, *93*, 9748–9753.
(23) Shapiro, S. D.; Kobayashi, D. K.; Ley, T. J. *J. Biol. Chem.* **1993**, *268*, 23824–23829.
(24) Li, W.; Li, J.; Wu, Y.; Rancati, F.; Vallese, S.; Raveglia, L.; Wu, J.; Hotchandani, R.; Fuller, N.; Cunningham, K.; Morgan, P.; Fish, S.; Krykbaev, R.; Xu, X.; Tam, S.; Goldman, S. J.; Abraham, W.; Williams, C.; Sypek, J.; Mansour, T. S. *J. Med. Chem.* **2009**, *52*, 5408–5419.
(25) Trott, O.; Olson, A. J. *J. Comput. Chem.* **2010**, *31*, 455–461.
(26) Bertini, I.; Calderone, V.; Cosenza, M.; Fragai, M.; Lee, Y.-M.; Luchinat, C.; Mangani, S.; Terni, B.; Turano, P. *Proc. Natl. Acad. Sci. U.S. A.* **2005**, *102*, 5334–5339.
(27) Hu, X.; Shelver, W. H. *J. Mol. Graphics Modell.* **2003**, *22*, 115–126.
(28) Dublanchet, A.-C.; Ducrot, P.; Andrianjara, C.; O'Gara, M.; Morales, R.; Compère, D.; Denis, A.; Blais, S.; Cluzeau, P.; Courté, K.; Hamon, J.; Moreau, F.; Prunet, M.-L.; Tertre, A. *Bioorg. Med. Chem. Lett.* **2005**, *15*, 3787–3790.
(29) Pirard, B.; Matter, H. *J. Med. Chem.* **2006**, *49*, 51–69.
(30) Morales, R.; Perrier, S.; Florent, J.-M.; Beltra, J.; Dufour, S.; De Mendez, I.; Manceau, P.; Tertre, A.; Moreau, F.; Compere, D.; Dublanchet, A.-C.; O'Gara, M. *J. Mol. Biol.* **2004**, *341*, 1063–1076.
(31) Bertini, I.; Calderone, V.; Fragai, M.; Luchinat, C.; Maletta, M.; Yeo, K. J. *Angew. Chem., Int. Ed.* **2006**, *45*, 7952–7955.
(32) Gabelloni, P.; Da Pozzo, E.; Bendinelli, S.; Costa, B.; Nuti, E.; Casalini, F.; Orlandini, E.; Da Settimo, F.; Rossello, A.; Martini, C. *Neuroscience* **2010**, *2*, 514–522.
(33) Rao, J. S. *Nat. Rev. Cancer* **2003**, *3*, 489–501.
(34) Uhm, J. H.; Dooley, N. P.; Villemure, J. G.; Yong, V. W. *Clin. Exp. Metastasis* **1996**, *14*, 421–433.
(35) Abe, T.; Mori, T.; Kohno, K.; Seiki, M.; Hayakawa, T.; Welgus, H. G.; Hori, S.; Kuwano, M. *Clin. Exp. Metastasis* **1994**, *12*, 296–304.
(36) Sarkar, S.; Nuttall, R. K.; Liu, S.; Edwards, D. R.; Yong, V. W. *Cancer Res.* **2006**, *66*, 11771–11780.
(37) Sivaparvathi, M.; Sawaya, R.; Chintala, S. K.; Go, Y.; Gokaslan, Z. L.; Rao, J. S. *Neurosci. Lett.* **1996**, *208*, 171–174.